# Vibrational properties of the one-component $\sigma$ phase

S.I.Simdyankin[1], S.N.Taraskin[2], M.Dzugutov[1], and S.R.Elliott[2]
[1] *Department of Numerical Analysis and Computing Science, Royal Institute of Technology, SE–100 44 Stockholm, Sweden.*
[2] *Department of Chemistry, University of Cambridge, Lensfield Road, Cambridge CB2 1EW, UK*
(February 1, 2008)

A structural model of a one-component $\sigma$-phase crystal has been constructed by means of molecular dynamics simulation. The phonon dispersion curves and the vibrational density of states were computed for this model. The dependence of the vibrational properties on the thermodynamical parameters was investigated. The vibrational density of states of the $\sigma$-phase structure is found to be similar to that of a one-component glass with icosahedral local order. On the basis of this comparison it is concluded that the $\sigma$ phase can be considered to be a good crystalline reference structure for this glass.

## I. INTRODUCTION

The local atomic order in disordered condensed materials is well defined and governs many physical properties[1]. Quite often, for a disordered marerial, it is possible to find a corresponding crystal with similar local and even intermediate-range order which give rise to similarities in many structural and dynamical features of these two solids. Such a crystal can be regarded as a reference crystalline structure (crystalline counterpart) for the corresponding disordered substance. In some cases, the reference structure can be uniquely defined. The simplest examples are toy structural models with force-constant and/or mass disorder. In these toy models, the atoms occupy their equilibrium positions at the sites of a crystalline lattice (e.g. simple cubic), which can be considered to be a reference one (see e.g.[2]). Another related example is a binary substitutional alloy, the reference system for which is a periodic point lattice with one of the two atomic species placed at the lattice sites[3]. The disorder in such models does not influence the equilibrium positions of the atoms arranged in an ideal crystalline lattice. This makes possible the use of approximate analytical approaches (e.g. the coherent potential approximation[3]) to treat the vibrational properties of the models, provided that the vibrational properties of the counterpart crystal are known.

In amorphous solids, or glasses, the atoms do not occupy the sites of a crystalline lattice, which results in positional disorder. For these materials, a choice of a reference structure becomes problematic. Good counterparts can usually be found among the crystalline polymorphs having the same (or similar) chemical composition as the corresponding glass. For example, $\alpha$-cristobalite appears to be a good crystalline counterpart for vitreous silica[4–6].

The main purpose of this paper is to investigate numerically the vibrational properties of a one-component $\sigma$-phase[7–9] crystal which is conjectured to be a good crystalline counterpart for a one-component glass with icosahedral local order (IC glass)[10,11].

The motivation for this choice of a crystalline counterpart of the IC glass is the following. The computational model of the IC glass is based on a simple empirical pair interatomic potential[10] resembling the effective interionic potentials conjectured for simple metallic glass-forming alloys[12]. The use of the same potential allows us to construct models of bcc and $\sigma$-phase crystals that are stable for a wide range of thermodynamical parameters[13]. Of these two crystalline structures, the $\sigma$ phase is expected to be a good reference structure for the IC glass because of the following reasons: The supercooled IC liquid (where the interactions between atoms are described by the same potential[10]) undergoes a transition either to the IC glass or to a dodecagonal quasicrystal[14] depending on the quench rate[13]. This quasicrystal has similar local structural properties with the IC glass[14]. However, the absence of global periodic order in the quasicrystalline phase makes the analysis of its vibrational properties a task of comparable complexity to that for the glass itself. The $\sigma$ phase is one of the closest low-order crystalline approximants[15] for this dodecagonal quasicrystal[16], which means that these two (crystalline and quasicrystalline) structures are built up from the same structural units. This implies that the IC glass and the $\sigma$ phase, being both tetrahedrally closed-packed structures[9], are nearly isomorphous in terms of local order.

Knowledge of the vibrational properties of the $\sigma$-phase crystal allows for a direct comparison with those of the IC glass. The apparent similarity in the vibrational densities of states of these two structures gives stronger support for the choice of this crystalline counterpart for the IC glass.

The $\sigma$-phase structure, used in our computations, has been obtained by means of molecular dynamics simulation with the use of an interatomic pair potential[10]. The vibrational properties have been investigated by using both a the normal-mode analysis and by computing the spectra of appropriate time-correlation functions.

The paper is arranged as follows: The $\sigma$-phase structure is described in Sec. II. The model and technical details of the calculations are presented in Sec. III. In Sec. IV we present the results of the simulations. Some concluding remarks are contained in Sec. V.

## II. THE $\sigma$ PHASE

In this Section, we review the known structural and dynamical properties of the $\sigma$ phase.

### A. Structure

The $\sigma$ phase belongs to an important class of tetrahedrally close-packed crystallographic structures[9], viz. the Frank-Kasper phases[7,8]. The first coordination shells of the constituent atoms in these structures form triangulated (Frank-Kasper) polyhedra composed entirely of slightly distorted tetrahedra. The four possible coordination numbers ($Z$) in these structures are $Z = 12, 14, 15$ and 16. The least distorted tetrahedra are found in icosahedra ($Z12$ polyhedra). Structures of small clusters of atoms interacting via pairwise central potentials favor icosahedral order[9] as having the lowest energy. The prototype $\sigma$ phase structures are $\beta$-U[17] and $Cr_{48}Fe_{52}$[18]. There are 30 atoms per tetragonal unit cell ($tP30$) with $c/a \approx 0.52$, where $c$ and $a$ are the dimensions of the cell (lattice parameters). The space group of this phase is $P4_2/mnm$. There are 10 atoms with the coordination number 12, $Z12$ or icosahedra, 16 $Z14$ atoms and 4 $Z15$ atoms. The $-72^\circ$ disclination lines[9] form a network (a major skeleton, in the parlance of Frank and Kasper[7,8]), where rows of $Z14$ atoms parallel to the tetragonal $c$-axis thread planar networks of $Z14$ and $Z15$ atoms. A projection of the $\sigma$-phase structure down the $c$-axis is shown in Fig. 1.

The Frank-Kasper phases share their significant geometrical property of icosahedral local order with simple metallic glasses[9,12]. Some liquid alloys which form Frank-Kasper phases have a tendency to freeze into metastable amorphous structures (metallic glasses) when quenched sufficiently rapidly[12]. It is now generally well accepted that, at least in the case of metallic alloys of simple constitution, glass formation is caused by the incompatibility of local icosahedral coordination with the translational symmetry in Euclidean space (geometrical frustration)[9]. There exist statistical mechanical arguments in favor of this scenario of glass formation[19] based on a Landau free-energy analysis. The average coordination number, $\overline{Z}$, in the Frank-Kasper phases ($13.333 \leq \overline{Z} \leq 13.5$) is very close to that of a sphere-packed "ideal glass" model[20] ($\overline{Z}_{\rm ideal} = 13.4$). In a sense, this "ideal glass" could be regarded as a Frank-Kasper phase with an infinitely large unit cell[9,20]. Thus the class of Frank-Kasper phases is a natural choice for reference crystalline structures for metallic glasses of simple constitution.

From a structural point of view, the $\sigma$ phase can be also regarded as a crystalline low-order approximant for dodecagonal quasicrystals[16]. Such quasicrystals[15], morphologically close to Frank-Kasper phases, represent an alternative class of noncrystallographic structures which combine icosahedral local order with non-translational long-range order manifested by infinitely sharp diffraction peaks.

### B. Dynamics

Similarities in the local structure of metallic glasses and Frank-Kasper phases are reflected in the dynamical properties of these materials.

The available data about the vibrational dynamics of Frank-Kasper phases is limited to some of the Laves phases, a subclass of the Frank-Kasper phases[12,21]. For instance, the similarity between the phonon-dispersion relations of the $Mg_{70}Zn_{30}$ glass[22,23] and those of the Laves phase $MgZn_2$[24] was emphasized by Hafner[12,25].

Another interesting aspect of the dynamics of Frank-Kasper phases is related to the appearance of soft vibrational modes in these materials. Such a soft low-frequency optic mode at the $\Gamma$-point (the origin of the reciprocal lattice) has been found numerically in the same Laves phase $MgZn_2$[24]. The frequency of this mode decreases with increasing pressure (accompanied by volume compression) and eventually becomes negative, indicating a structural phase transition[26–30]. The authors of Ref.[24] applied a group-theoretical analysis and demonstrated that the polarization vector of the soft optic mode in $MgZn_2$ is determined by the structure symmetry and is independent of interatomic interactions. This suggests that the soft-mode character of some vibrations is a generic property of Frank-Kasper phases. However, no soft-mode behavior was observed in the isostructural $CaMg_2$[31] where the mass ratio of the

constituent elements is reversed with respect to $MgZn_2$. Hafner[12] suggested that the soft modes in $MgZn_2$ should be attributed to the relatively large mass of the Zn atoms. This is an example of the chemical composition of the materials introducing considerable difficulties into the analysis of the interplay of the structure and the dynamics.

A numerical simulation of a one-component Frank-Kasper phase allows us to eliminate this uncertainty. We investigate the behavior of the lowest-frequency optic modes in the one-component $\sigma$ phase with variable pressure in Sec. IV B 3.

## III. METHODS OF COMPUTATION

We have constructed a thermodynamically stable structural model of the one-component $\sigma$ phase by means of classical molecular dynamics simulation. In this case, success strongly depends on the choice of the interatomic potential for the model. For example, the Lennard-Jones potential, widely used in creating simple models of liquids[32], glasses[33], and crystals[34], is not suitable for this purpose, because the $\sigma$ phase is not stable for it in the range of thermodynamical parameters investigated below (the stable phase is the fcc lattice). Instead, we use a pair interatomic potential suggested in Ref.[10] and show that it is possible to construct a one-component $\sigma$ phase which is stable for a wide range of thermodynamical parameters[13].

### A. Model

As a mathematical model for the study of atomic dynamics in the crystalline $\sigma$-phase structure, we consider a classical system of $N$ identical particles interacting via a spherically symmetric pair potential.

The pair potential used in this study[10] is designed to favor icosahedral local order. The main repulsive part of this potential is identical to that of the Lennard-Jones potential $u_{\rm LJ}(r) = 4\epsilon[(\sigma/r)^{12} - (\sigma/r)^6]$; therefore all the quantities in these simulations are expressed in reduced Lennard-Jones units[35], i.e. with $\sigma$, $\epsilon$, and $\tau_0 = (m\sigma^2/\epsilon)^{1/2}$ chosen as length, energy, and time units. To convert the reduced units to physical units one can refer to argon ($m = 39.948$ a.m.u.) by choosing the Lennard-Jones parameters $\sigma = 3.4$ Å and $\epsilon/k_B = 120$ K. In this case, our frequency unit $\nu_0 = \tau_0^{-1}$ corresponds to 0.4648 THz. The analytical expression defining the potential is given in Ref.[10]. This potential resembles those for simple glass-forming metallic alloys[12] with only the first of the Friedel oscillations being retained (see Fig. 2).

We use conventional molecular dynamics simulations[35] in which the Newtonian equations of motion are solved using a finite-difference algorithm with time step equal to 0.01 while the particles are enclosed in a simulation box of volume $V$ with periodic boundary conditions. In this case, the total energy $E$ is a constant of motion and time averages obtained in the course of simulations approximate the ensemble averages in the microcanonical (constant-$NVE$) statistical ensemble. Wavevectors,

$$\mathbf{Q} = n_x\mathbf{Q}_{x,0} + n_y\mathbf{Q}_{y,0} + n_z\mathbf{Q}_{z,0} \tag{3.1}$$

with $n_x$, $n_y$ and $n_z$ being integers, compatible with periodic boundary conditions are multiples of the three fundamental wavevectors $\mathbf{Q}_{x,0} = \frac{2\pi}{L_x}(1,0,0)$, $\mathbf{Q}_{y,0} = \frac{2\pi}{L_y}(0,1,0)$ and $\mathbf{Q}_{z,0} = \frac{2\pi}{L_z}(0,0,1)$, where $L_x$, $L_y$, and $L_z$ are the dimensions of the (tetragonal) simulation box. In order to have a sufficient number of allowed wavevectors within the Brillouin zone, the sample dimensions must be sufficiently large. The time-correlation functions resulted from the molecular dynamics simulation reported below were obtained for a system of 20580 particles ($7 \times 7 \times 14$ unit cells with 30 atoms per unit cell). This relatively large system size also gives sufficient statistical accuracy[36]. Where necessary, we performed simulations in other ensembles by modifying the equations of motion[37,38].

The arrangement of atoms in a unit cell of the model $\sigma$-phase structure used in our computer simulations is shown in fig. 1(b). The optimal (with respect to an energy minimization) $c/a$ ratio was taken to be equal to 0.5273. To determine the optimal model structure, it was sufficient to perform molecular dynamics simulations with the number of particles in the system equal to $N = 1620$ ($3\times3\times6$ unit cells). Details of the preparation of this atomic configuration are given in section IV A.

### B. Time-correlation functions

A straightforward method to analyze the vibrational dynamics in a molecular dynamics model is to imitate inelastic neutron scattering experiments by calculating the dynamical structure factor $S(\mathbf{Q},\omega)$[34], proportional to the neutron scattering cross-section[27,32], which is the spectrum of the density autocorrelation function:

$$F(\mathbf{Q},t) =< \rho(\mathbf{Q},t)\rho(-\mathbf{Q},0) > \tag{3.2}$$

where

$$\rho(\mathbf{Q},t) = \sum_{k=1}^{N} \exp(-i\mathbf{Q}\cdot\mathbf{r}_k(t)) \tag{3.3}$$

is the Fourier transform of the local particle density[32], $N$ is the number of particles in the system, $\mathbf{r}_k(t)$ is the position vector of particle $k$, and the wavevector $\mathbf{Q}$ takes on the values according to Eq. (3.1). A longitudinal phonon is associated with a maximum in $S(\mathbf{Q},\omega)$ at a fixed $\mathbf{Q}$. In order to get information about the transverse modes from $S(\mathbf{Q},\omega)$, one has to select wavevectors outside the first Brillouin zone[39].

In a more convenient way, the vibrational modes can be studied using the current autocorrelation function[32]:

$$C_{\mathbf{e}}(\mathbf{Q},t) = \frac{Q^2}{N} < j_{\mathbf{e}}(\mathbf{Q},t) j_{\mathbf{e}}(-\mathbf{Q},0) > \tag{3.4}$$

where

$$j_{\mathbf{e}}(\mathbf{Q},t) = \sum_{k=1}^{N} (\mathbf{e}\cdot\mathbf{v}_k(t)) \exp[-i\mathbf{Q}\cdot\mathbf{r}_k(t)] \tag{3.5}$$

is the Fourier transform of the local current, $\mathbf{v}_k(t)$ is the velocity of particle $k$, and $\mathbf{e}$ is the unit polarization vector.

Note that for the longitudinal polarization, $\mathbf{e} \parallel \mathbf{Q}$, Eq. (3.4) can be obtained from (3.2) by double differentiation with respect to time. For the transverse-current correlation functions, the polarization vector must be chosen consistently with the lattice symmetry.

At a temperature $T$, the vibrational density of states $g(\omega)$ can be calculated as the Fourier transform of the normalized velocity autocorrelation function[26,33]:

$$Z(t) = \frac{1}{3NT} \left\langle \sum_{k=1}^{N} \mathbf{v}_k(t)\cdot\mathbf{v}_k(0) \right\rangle \tag{3.6}$$

We computed the time-correlation functions using the overlapped data collection technique[40]. The number of overlapped measurements used for statistical averaging was about 10000. The time origins of the measurements were separated by 0.2 r.u. (20 time steps).

In order to reduce the finite-time truncation effects in the spectra of the time-correlation functions, we used a Gaussian window function with the half-width equal to 3 r.u.

### C. Normal-mode analysis

To calculate the dispersion relations in the harmonic approximation, we used the standard method based on diagonalization of the Fourier transformed dynamical matrix[41]. From the known dispersion relations, $\omega_s(\mathbf{Q})$, $s = 1, 2, \ldots, 90$, the vibrational density of states can be computed by integration over the first Brillouin zone according to

$$g(\omega) = \frac{v}{r(2\pi)^3} \sum_{s=1}^{r} \int_{\mathrm{BZ}} \delta(\omega - \omega_s(\mathbf{Q}))\, d\mathbf{Q} \tag{3.7}$$

where the sum is over all $r$ dispersion branches and $v$ stands for the volume of the unit cell. In the computations, a Gaussian function with small but finite width is substituted for the $\delta$-function. The half-width of the Gaussian function in our computations was equal to about 0.05. Formally, the wavevector $\mathbf{Q}$ in Eq. (3.7) is a continuous variable, but in the simulations the integral was estimated by a sum over a uniform rectangular grid of $100\times100\times100$ points in the first Brillouin zone.

## IV. RESULTS

### A. Optimization of the structure in the $\sigma$ phase

In this subsection, we describe the method of construction of the thermodynamically stable model of the $\sigma$ phase and analyse the range of its stability.

There are several ways to obtain numerical values of the atomic coordinates in the $\sigma$ phase. One way is to use those available for $Cr_{48}Fe_{52}$[42]. Alternatively, a unit cell of the $\sigma$-phase structure can be constructed either by manipulating the kagomé tiling according to the algorithm given by Frank and Kasper in ref.[8] or by stacking the square and triangular basic elements of the dodecagonal quasicrystal model[16,43] into the $3^2, 4, 3, 4$ square-triangle net[8] (see fig. 1(a)). The arrangements of the atoms resulting from these constructions do not correspond exactly, although the difference is rather small – the root-mean-square distance between the corresponding atoms in different configurations is of the order of a few percent of the root-mean-square distance between different atoms in the same configuration. In either case, the resulting structure is an approximate one in the sense that the atomic positions do not correspond to a minimal potential-energy configuration for a given interaction potential. To obtain the true structure corresponding to the potential, the approximate configuration must be relaxed by a molecular dynamics program. Moreover the $c/a$ ratio is slightly different for different natural $\sigma$-phase crystals, which means that this ratio is not uniquely defined.

The atomic configuration of the $\sigma$ phase used in this study was prepared as follows. A sample of $N = 1620$ particles ($3 \times 3 \times 6$ unit cells) was constructed by filling a tetragonal box of appropriate dimensions with $\sigma$-phase unit cells. We used the unit-cell atomic configuration suggested by Gähler[16,43] with $c/a = 0.5176$. The number density, $\rho = N/V$, $V = L_x L_y L_z$, of this atomic configuration was $\rho = 1.0048$. This configuration was then used to provide the initial atomic coordinates for variable-shape $NST$ (constant number of atoms, pressure tensor, and temperature) molecular dynamics[38], the run performed at $S = 0$ and $T = 0$. This procedure is equivalent to a potential-energy minimization by the steepest descent method under the condition of independent pressure balance in each spatial dimension. The variable-shape $NST$ run resulted in an ideal crystalline structure for which the fractional coordinates of the atoms in all unit cells were identical within the precision of the calculations. The structure of the $\sigma$ phase thus obtained is characterized by the minimum potential energy per atom, $U_{\min} = -2.5899$, with respect to variations of thermodynamical parameters. In order to check this, we have performed similar $NST$ runs at different pressures and indeed found that the energy is minimum at zero pressure (see Fig. 3a,b). The density for the optimal structure has been found to be $\rho = 0.8771$ and the ratio of the lattice parameters is $c/a = 0.5273$, close to that of $\beta$-U ($c/a = 0.5257$, at $T = 720°C$)[44]. The potential-energy minimum for the bcc structure at the same density with the same potential was $U_{\min} = -2.6148$. At zero pressure, the density of the bcc structure is $\rho = 0.8604$ and the minimum potential energy per atom is $U_{\min} = -2.6357$, i.e. in both cases lower than for the $\sigma$ phase. It was shown earlier[13] that the potential energy per atom for the $\sigma$ phase becomes lower than that for the bcc structure at the same density as the temperature increases. This is consistent with the fact that natural crystalline $\sigma$ phases are stable only at high temperatures. They undergo a solid-solid phase transition to a simpler crystalline phase as the temperature decreases. In our simulations, however, the system was stable in the range of temperatures $T \lesssim 0.9$ for as long as $t_{\text{run}} = 5000$.

We have also investigated the thermodynamical stability of the $\sigma$ phase under variable pressure. We have found that the $\sigma$ phase is stable for pressures in the range $-5 \lesssim P \lesssim 12$. At high pressures $P \gtrsim 12$, a structural transformation occurs, resulting in the fcc structure. The phase diagram of the IC potential is not known at present. We can expect that at densities greater than the triple-point density for the Lennard-Jones system, $\rho \approx 0.85$[32], the solid-fluid coexistence curve for the IC system is close to that for the LJ system. We can only estimate that the melting temperature at $\rho = 0.8771$ is about $0.8 \lesssim T \lesssim 0.9$ from the fact that the $\sigma$-phase crystalline structure is stable at $T = 0.8$ on the time scale of our computations. No diffusion was observed at temperatures up to $T = 0.8$. At $T = 0.9$ the system stayed in a metastable superheated state for about $t_{\text{run}} = 5000$, after which it melted.

We used the density and the $c/a$ ratio obtained from the $NST$ run to perform $NVE$ (constant number of atoms, volume, and total energy) molecular dynamics runs starting from the three configurations mentioned above and scaling the velocities to zero at each time step, which is also equivalent to a potential-energy minimization by the steepest-descent method. The same was done for one instantaneous configuration corresponding to the temperature $T = 0.8$. The configurations resulting from this procedure were identical, which is an indication that there is a well-defined potential-energy minimum corresponding to a unique crystallographic arrangement of atoms within the $\sigma$-phase unit cell. This structure, scaled so that $a = c = 1$, is shown in fig. 1(b). The atomic layers with $z$ close to 0.25 and 0.75, which are not closely packed, show a small but significant puckering – an effect present in the $\beta$-U[17] and $Cr_{48}Fe_{52}$[42] structures.

### B. Vibrational dynamics

Above, we have discussed the similarities in the local structure of the $\sigma$ phase and the IC glass. These similarities are expected to cause the vibrational spectra in these two materials also to be similar. In order to check this assumption, in this subsection we investigate the vibrational properties of the $\sigma$ phase and compare the vibrational spectra of this crystal and the IC glass.

If the vibrational spectra are similar, the $\sigma$ phase can be considered to be a good crystalline reference structure for the IC glass. One consequence of these similarities is that we can use the data about the vibrational properticies of the $\sigma$ phase crystal to explain the nature of the vibrational excitations in the corresponding amourphous structure.

#### *1. Phonon dispersion in the $\sigma$ phase*

The $\sigma$ phase has 30 atoms per unit cell which result in 3 acoustic and 87 optic branches, as shown in Fig. 4. The vibrational density of states (VDOS) obtained by integration over the first Brillouin zone (see Eq. (9)) is shown on the right-hand side of Fig. 4. The linear dispersion of the acoustic branches in the low-frequency range ($\omega \lesssim 4$) results in the Debye law for the VDOS, $g(\omega) = 3\omega^2/\omega_{\rm D}^3$, with the Debye frequency equal to $\omega_{\rm D} \approx 23.89$. The Debye frequency has been estimated from a fit of the initial part of the VDOS by a parabolic function. The optic branches are densely distributed above the acoustic part. There are no large gaps in the spectrum, which is a consequence of tight binding and the mutual penetration of the basic structural units (Frank-Kasper polyhedra) in the $\sigma$ phase. In other words, there are no isolated structural units, like molecules in molecular crystals[26] and crystalline fullerens[45], or tetrahedra in silica[5], the vibrations of which form separate optic bands. At some of the zone boundaries (e.g. the X point; see Fig. 4) the dispersion curves do not show zero derivatives. This is because the space group $P4_2/mnm$ of the $\sigma$ phase is nonsymmorphic, i.e. it contains nonpoint symmetry elements involving fractional translations[26,46].

#### *2. Comparison with the IC glass*

An informative characteristic of the vibrational dynamics in the IC glass which can be compared with the $\sigma$ phase is its VDOS[47] (see Fig. 5) which can be easily obtained from the velocity autocorrelation function Eq. (3.6). The VDOS for the bcc lattice is also presented for comparison in the figure (the dashed line). We can clearly see that the frequency range of the whole spectrum is the same for the $\sigma$ phase and the IC glass but differs for the bcc lattice. The shape of the IC-glass spectrum mainly reproduces the basic features of the $\sigma$ phase spectrum and can be imagined as a superposition of broadened (by disorder) crystalline peaks. This is a consequence of the presence of a large number of optic modes in the vibrational spectrum of the sigma-phase structure located in the same frequency region as the whole spectrum of the IC glass. Therefore, the similarities in the VDOS of the $\sigma$ phase and the IC glass strongly support the choice of the $\sigma$ phase as a crystalline counterpart.

#### *3. Soft modes in the $\sigma$ phase*

As was mentioned in Sec. II B, an interesting feature of atomic dynamics in the Frank-Kasper phases is related to the appearance of low-frequency soft modes. We have investigated whether a soft mode appears in our model of the $\sigma$-phase structure. For this purpose, we followed the evolution of the vibrational spectrum with variable pressure (see Fig. 6 and, indeed, found that one of the lowest-frequency optic modes (doubly degenerate) in the $\Gamma$-point shows soft-mode behavior. The frequency of this mode decreases both with decreasing and increasing pressure (see Fig. 7). The decrease of the mode frequency at negative pressures is not surprising and reflects the softening of the whole vibrational spectrum (see Fig. 6a). However, with increasing pressure, the whole spectrum is shifted to higher frequencies (see Fig. 6c), while the frequency of the soft mode (a small peak around $\omega = 3.5$ in Fig. 6c) moves in the opposite direction, approaching zero and thus indicating a structural instability (structural phase transition to the fcc lattice) at a critical pressure $P_* \approx 12.5$ (see Fig. 7). Around this value of the pressure the structure of the $\sigma$ phase becomes extremely unstable and an investigation of the details of atomic motion requires a thorough analysis. We hope to address this point in another study.

### 4. Anharmonicity in the $\sigma$ phase

One of the interesting questions concerning the vibrational dynamics of the $\sigma$ phase is related to the range of applicability of the harmonic approximation for the lattice vibrations. We are able to anwer this question by investigating the vibrational spectrum using the velocity autocorrelation function with increasing temperature and comparing it with the results of the normal-mode analysis (harmonic approximation).

To assess the degree of temperature-induced anharmonicity, we computed the dispersion relations for the symmetry direction [001] ($\mathbf{Q} \parallel \mathbf{c}$, $\Gamma$Z in Fig. 4) at different temperatures by using both these techniques (molecular dynamics and normal-mode analysis) and compared the results. These are shown in Fig. 8 for several low- and high-frequency dispersion branches for two temperatures $T = 0.01$ and $T = 0.8$. At intermediate frequencies, the density of dispersion branches is so high that a comparison between the results of the two methods of calculation of dispersion relations is hardly possible, mainly because of the finite width of the respective peaks in the spectra of the current autocorrelation functions (see sec. III B). Due to the fact that the $\sigma$-phase space group $P4_2/mnm$ is nonsymmorphic, i.e. it contains nonpoint symmetry elements involving fractional translations[46], the phonon-dispersion relations, derived from the peak positions in $C_l(\mathbf{Q},\omega)$ and $C_t(\mathbf{Q},\omega)$, appear in the extended zone scheme[26]. The optic modes cannot be measured in the vicinity of the origin of the first Brillouin zone $Q = 0$ ($Q = |\mathbf{Q}|$), because this long-wavelength limit corresponds to motion of the system as a whole, forbidden by the periodic boundary conditions. Information about these modes is available at the boundaries ($Q = 2\pi/c, 6\pi/c$) and at the origin ($Q = 4\pi/c$) of the second extended Brillouin zone. The molecular dynamics results for the dispersion relations at $T = 0.01$ are adapted from the second extended Brillouin zone. To make possible the comparison with the results obtained in the harmonic approximation, the data in the region $Q \in [5\pi/c, 6\pi/c]$ were folded with respect to $Q = 5\pi/c$ into the region $Q \in [4\pi/c, 5\pi/c]$, which corresponds to half of an irreducible zone. From these results we can see that the harmonic approximation works quite well at the low temperature of $T = 0.01$. At $T = 0.8$, only the acoustic branches could be resolved without ambiguity. Therefore, for this temperature, we used the data available from the first Brillouin zone.

One important signature of temperature-induced anharmonicity is a softening of the acoustic modes, i.e. a lowering of the acoustic branches with respect to those calculated in the harmonic approximation which occurs as the temperature increases[26]. This effect can be clearly seen for $T = 0.8$ in Fig. 8. In accordance with this observation, the vibrational density of states for this temperature, shown in Fig. 9, exhibits the presence of excess states with respect to the harmonic approximation. A deviation from the harmonic approximation in $g(\omega)$ at low frequencies (see the inset in Fig. 9) starts to be noticeable at a temperature of about $T = 0.2$. Therefore, we can conclude the the lattice dynamics in the $\sigma$ phase is harmonic in a wide range of temperatures $T \lesssim 0.2$.

Finally, we would like to note the similarity between the high-temperature VDOS for the $\sigma$ phase and the low-temperature VDOS for the IC glass (see Fig. 10). Since $g(\omega)$ for the glass is only slightly temperature dependent, we show it only for $T = 0.01$. The fact that the densities of states for the glass and the high-temperature $\sigma$ phase in fig. 10 are remarkably similar clearly indicates that the effect of the thermally-induced dynamical disorder in the crystalline structure on the vibrational spectrum is similar to that of the configurational disorder characteristic of the amorphous structure.

## V. CONCLUSIONS

In this paper we have studied the structural and vibrational properties of a $\sigma$-phase crystal. First, we have shown that it is possible to construct a structural model of a one-component $\sigma$ phase by means of molecular dynamics simulations using an appropriate pair potential. This $\sigma$-phase structure is stable in a wide range of thermodynamical parameters. Our model of the $\sigma$ phase contains only one atomic component. This is important in understanding the role of topological icosahedral order alone on the structural and dynamical properties and avoids the effects arising from the presence of different atomic species.

Second, we have investigated atomic vibrational dynamics of the $\sigma$ phase. In particular, we have found the range of applicability of the harmonic approximation in a description of atomic dynamics. We have also demonstrated the existence of soft modes in the $\sigma$ phase which leads to a structural phase transformation with increasing pressure.

Third, we have demonstrated that the $\sigma$ phase is a good crystalline counterpart of the IC glass. This has been done on the basis of a comparative analysis of the vibrational dynamics (vibrational density of states).

We think that the results on the vibrational properties of the $\sigma$ phase discussed above can be used in an analysis of the peculiar vibrational properties of the IC glass (e.g. the Boson peak[5]). We also believe that the computational data of the vibrational properties of the $\sigma$ phase could be of value for metallurgy where this phase has received much detailed attention, chiefly because of the detrimental effect which the formation of this phase has on mechanical properties of certain steels[48].

**ACKNOWLEDGEMENTS**

S.I.S. and M.D. thank Trinity College for hospitality. We are grateful to H.R. Schober for bringing to our attention Ref.[28].

---

[1] S.R. Elliott, *Physics of Amorphous Materials* 2nd Edn. (Longman, N.Y., 1990).
[2] W. Schirmacher, G. Diezemann, and C. Ganter, *Phys. Rev. Lett.* **81** (1998) 136-139.
[3] H. Ehrenreich and L.M. Schwarts, in *Solid State Physics* Ed. by H. Ehrenreich, F. Seitz and D. Turnbull (Academic, NY, 1976) Vol. 31, p. 149-286.
[4] Y. Ding, T. Nanba, and Y. Miura, *Phys. Rev. B* **58** (1998) 14279-14287.
[5] S.N. Taraskin and S.R. Elliott, *Phys. Rev. B* **56** (1997) 8605-8622.
[6] M.T.Dove, M.J.Harris, A.C.Hannon, J.M.Parker, I.P.Swainson, and M.Gambhir, *Phys. Rev. Lett.* **78** (1997) 1070.
[7] F.C. Frank and J.S. Kasper, *Acta Cryst.* **11** (1958) 184-190.
[8] F.C. Frank and J.S. Kasper, *Acta Cryst.* **12** (1959) 483-499.
[9] D.R. Nelson and F. Spaepen, *Solid State Phys.* **42** (1989) 1-90.
[10] M. Dzugutov, *Phys. Rev. A* **46** (1992) R2984-R2987.
[11] M. Dzugutov, *J. Non-Cryst. Sol.* **156&158** (1993) 173-176.
[12] J. Hafner, *From Hamiltonians to Phase Diagrams* (Springer-Verlag, Berlin, 1987)
[13] M. Dzugutov, *Phys. Rev. Lett.* **79** (1997) 4043.
[14] M. Dzugutov, *Phys. Rev. Lett.* **70** (1993) 2924-2927.
[15] C. Janot, *Quasicrystals: a Primer* (Oxford University Press, Oxford, 1994)
[16] J. Roth and F. Gähler, *Eur. Phys. J. B* **6** (1998) 425-445.
[17] A.C. Lawson, C.E. Olsen, J.W. Richardson Jr, M.H. Mueller, and G.H. Lander, *Acta Cryst. B* **44** (1988) 89-96.
[18] H.L. Yakel, *Acta Cryst. B* **39** (1983) 20-33.
[19] S. Sachdev and D.R. Nelson, *Phys. Rev. B* **32** (1985) 1480-1502.
[20] D.R. Nelson, *Phys. Rev. B* **28** (1983) 5515-5535.
[21] W. Kress, *Phonon dispersion curves, one-phonon densities of states and impurity vibrations of metallic systems* (Physics Data, Karlsruhe: Fachinformationszentrum Karlsruhe, 1987)
[22] J.-B. Suck and H. Rudin, in *Glassy Metals II* edited by H.J. Güntherodt and H. Beck, Topics in Applied Physics (Springer-Verlag, Berlin, 1983), p.217-260.
[23] J.-B. Suck, P.A. Egelstaff, R.A. Robinson, D.S. Sivia, and A.D. Taylor, *Europhys. Lett.*, **19** (1992) 207-213.
[24] H. Eschrig, K. Feldman, K. Hennig, and L. Weiss, *Neutron Inelastic Scattering* (IAEA, Wien, 1972), p.157-171.
[25] J. Hafner, *J. Phys. C* **16** (1983) 5773-5792.
[26] M.T. Dove, *Introduction to Lattice Dynamics* (Cambridge University Press, Cambridge, 1993)
[27] N.W. Ashcroft and N.D. Mermin, *Solid State Physics* (Saunders College, Philadelphia, 1976), p.456.
[28] A. Heiming, W. Petry, J. Trampenau, M. Alba, C. Herzig, H.R. Schober, and G. Vogl, *Phys. Rev. B* **43** (1991) 10948-10962.
[29] B.L. Zhang, C.Z. Wang, K.M. Ho, D. Turner, and Y.Y. Ye, *Phys. Rev. Lett.* **74** (1995) 1375-1378.
[30] R. Meyer and P. Entel, *Phys. Rev. B* **57** (1998) 5140-5147.
[31] H. Eschrig, K. Feldman, K. Hennig, W. Matz, and P. Paufler, *Phys. Stat. Sol. B* **79** (1977) 283-288.
[32] J.-P. Hansen and I.R. McDonald, *Theory of Simple Liquids* (Academic Press, London, 1986), p.221.
[33] M. Sampoli, P. Benassi, R. Dell'Anna, V. Mazzacurati, and G. Ruocco, *Philosophical Magazine B* **77** (1998) 473-484.
[34] M.L. Klein, in *Computer Modeling of Matter*, edited by P. Lykos, (ACS, Washington, 1978), p.94-110.
[35] M.P. Allen and D.J. Tildesley, *Computer Simulation of Liquids* (Clarendon Press, Oxford, 1987), p.327.
[36] M. Dzugutov, *Material Science and Engineering A* **134** (1991) 921-926.
[37] D. Frenkel and B. Smit, *Understanding Molecular Simulation* (Academic Press, San Diego, 1996)
[38] W. Smith and T. Forester, *J. Molec. Graphics* **14** (1996) 136-141.
[39] H.R. Schober and W.Petry, in *Structure of Solids*, edited by V. Gerod, Material Science and Technology, Vol. 1 (VCH, Weinheim, 1993), p.346.
[40] D.C. Rapaport, *The Art of Molecular Dynamics Simulation* (Cambridge University Press, Cambridge, 1995)
[41] A.A. Maradudin, E.W. Montroll, G.H. Weiss, and I.P. Ipatova, *Theory of Lattice Dynamics in the Harmonic Approximation*, Solid State Physics, Supplement 3 (Academic Press, New York, 1971)
[42] J.L.C. Daams, P. Villars, and J.H.N. van Vucht, *Atlas of Crystal Structure Types for Intermetallic Phases* (ASM International, Materials Park, OH, 1991), p.3804.
[43] F. Gähler, private communication.
[44] J. Thewlis, *Acta Cryst.* **5** (1952) 790-794.

[45] J. Yu, R.K. Kalia, and P. Vashishta, *Appl. Phys. Lett.* **63** (1993) 3152-3154.
[46] W. Steurer, in *Structure of Solids*, edited by V. Gerod, Material Science and Technology, Vol. 1 (VCH, Weinheim, 1993), p.37.
[47] M. Dzugutov, *Physica A* **201** (1993) 430-433.
[48] T.B. Massalski, in *Physical Metallurgy*, edited by R.W. Cahn and P. Haasen, Vol. 1 (North-Holland, Amsterdam, 1996), p.178.

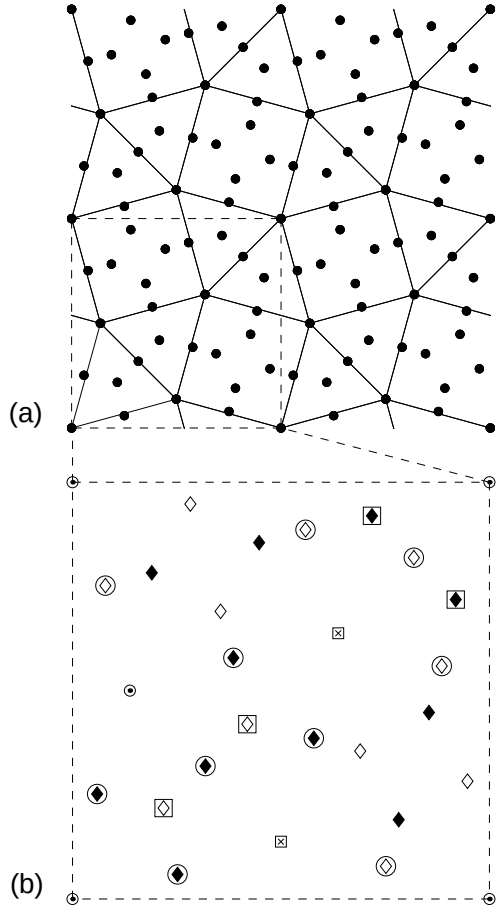


FIG. 1. Projection down the $c$-axis of the $\sigma$-phase structure: (a) $3^2, 4, 3, 4$ net (the numerical symbols are Schläfli symbols[7], specifying the number and sequence of various polygons around each vertex). The dashed square outlines a unit cell; (b) Atomic arrangement in one unit (cubic) cell. ◊: $z = 0$, ⧫: $z = 0.5$, •: $z = 0.2499$. ×: $z = 0.2501$, ○: $z = 0.7499$, □: $z = 0.7501$, ◯: Z12 atoms, ☐: Z15 atoms. The rest of atoms are Z14. Multiplying $z$ by the proper $c/a$ ratio gives a tetragonal unit cell with $a = 1$.

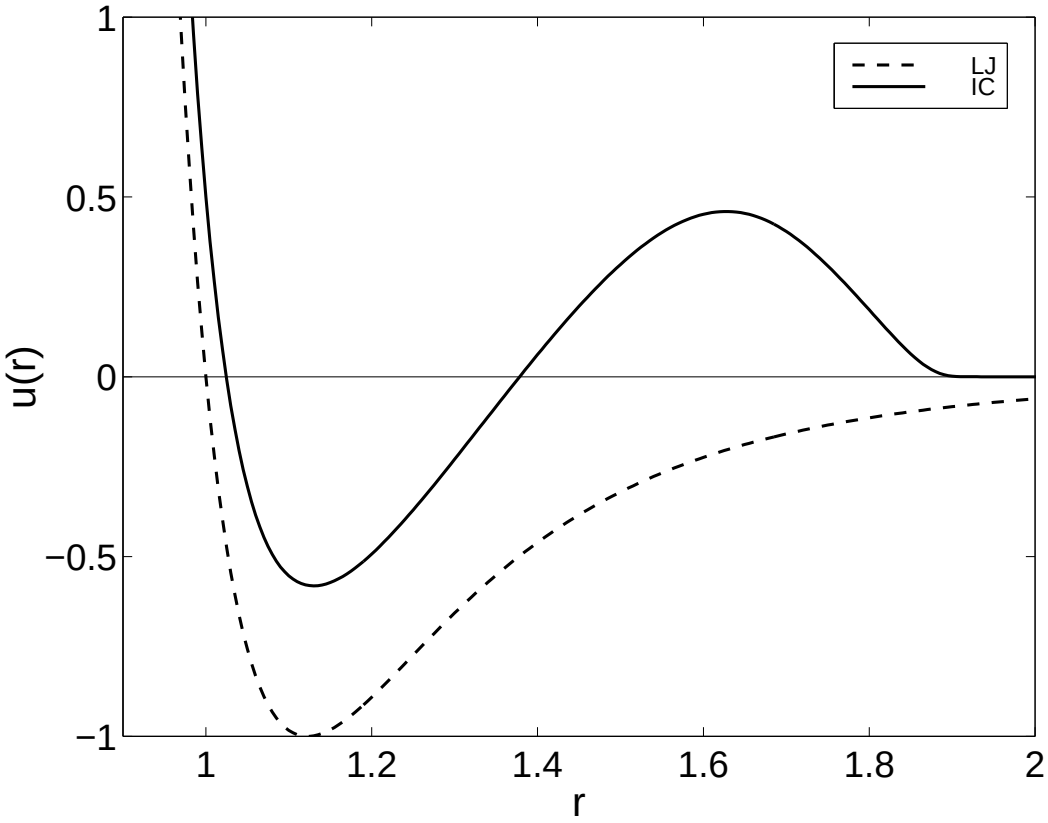


FIG. 2. The IC pair potential used in this study[10] (solid line) compared with the Lennard-Jones potential (dashed line).

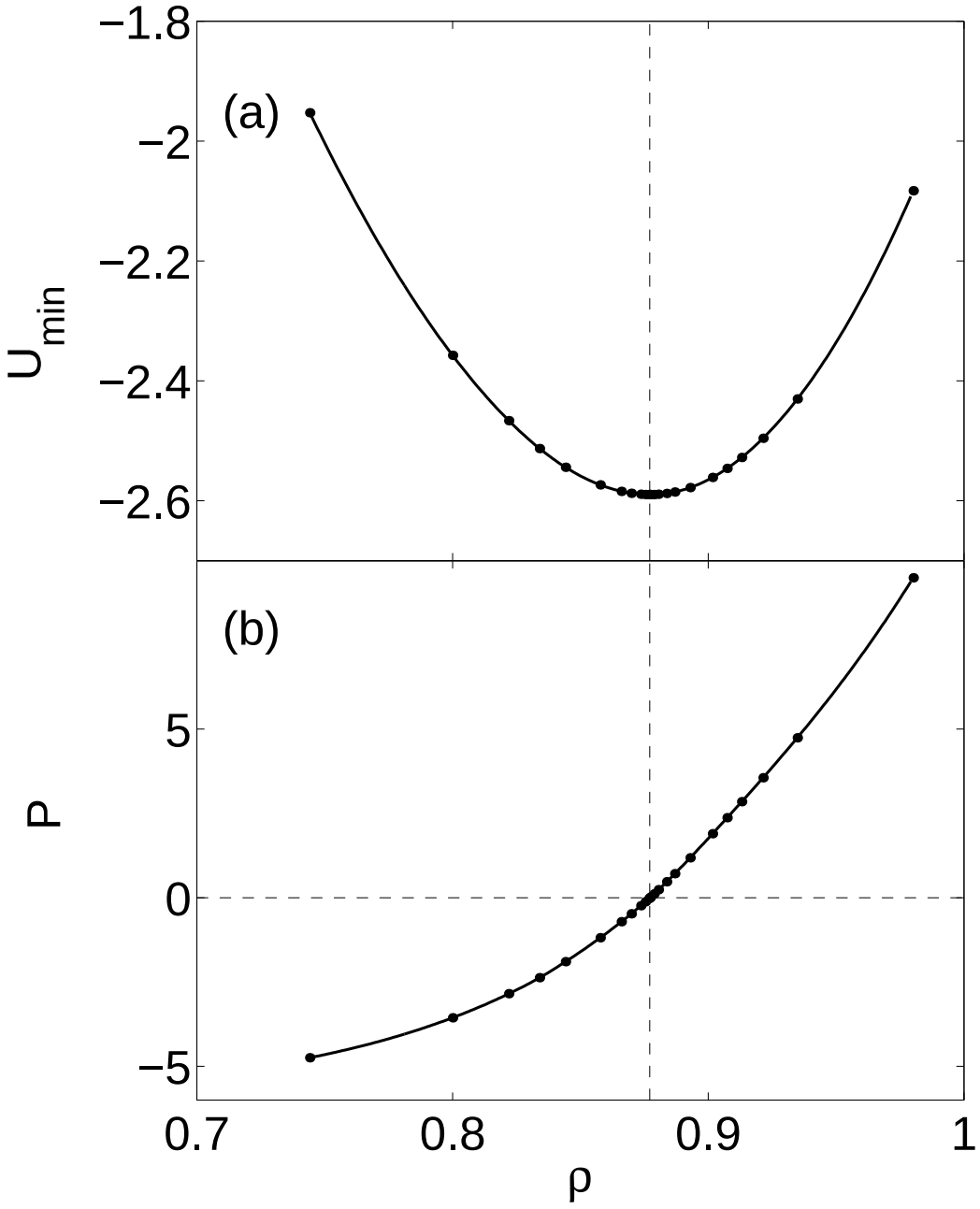


FIG. 3. (a) Minimal potential energy of the $\sigma$-phase structure as a function of density. (b) Pressure as a function of density. The dots show the data points and the solid curves are obtained by a cubic interpolation.

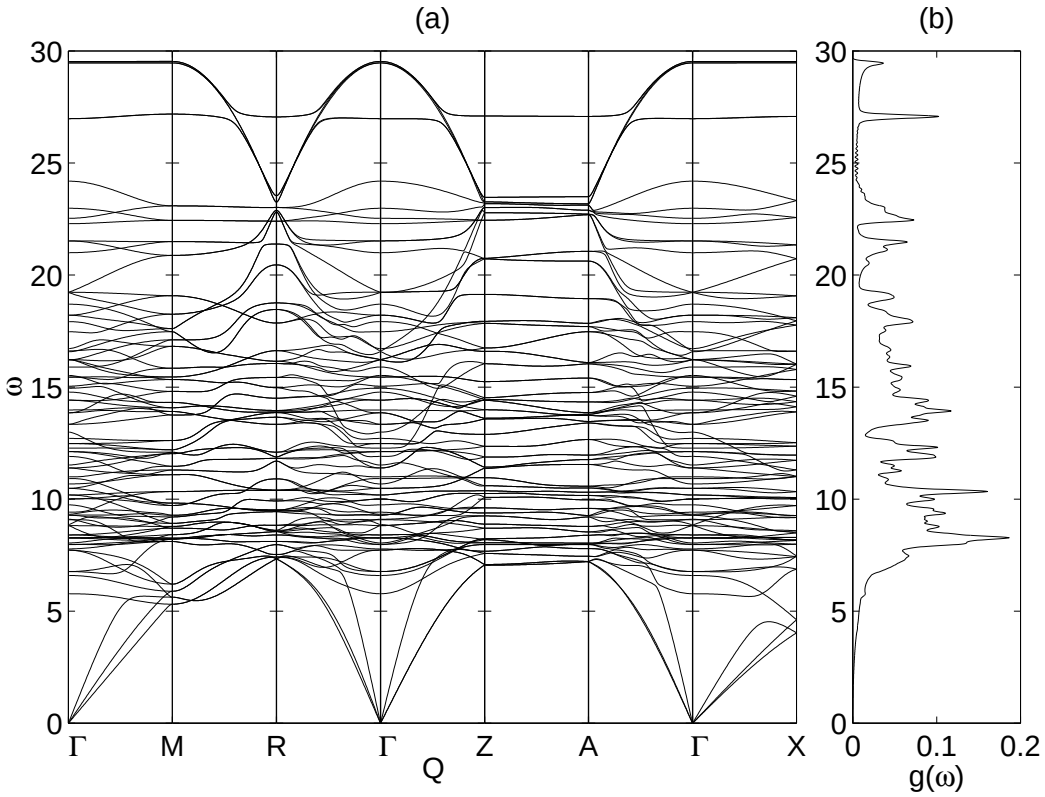


FIG. 4. Phonon-dispersion relations along the symmetry directions (a) and vibrational density of states (b) evaluated by a normal-mode analysis in the harmonic approximation. The symmetry points on the surface of the first Brillouin zone are $\Gamma = (0,0,0)$, $\mathrm{M} = (\frac{\pi}{a}, \frac{\pi}{a}, 0)$, $\mathrm{R} = (\frac{\pi}{a}, \frac{\pi}{a}, \frac{\pi}{c})$, $\mathrm{Z} = (0,0,\frac{\pi}{c})$, $\mathrm{A} = (\frac{\pi}{a}, 0, \frac{\pi}{c})$, $\mathrm{X} = (\frac{\pi}{a}, 0, 0)$.

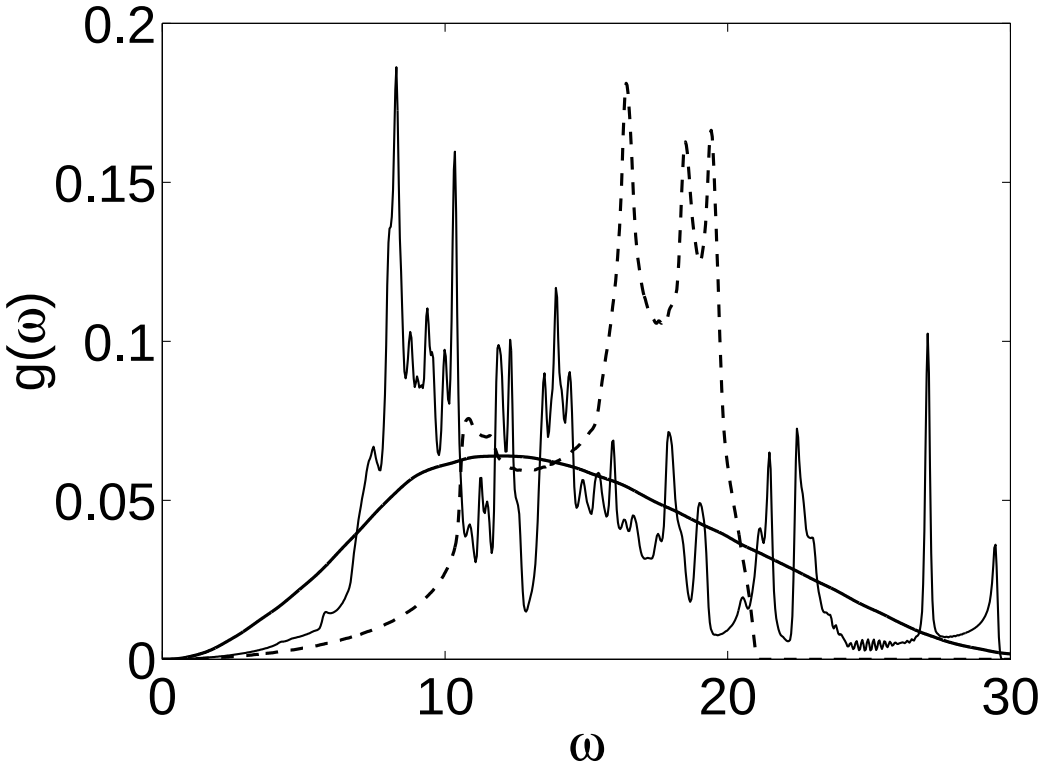


FIG. 5. Vibrational densities of states calculated by a normal-mode analysis for the $\sigma$-phase (thin solid line) and for bcc (dashed line) structures, and from the velocity autocorrelation function for the IC glass (thick solid line) at the temperature $T = 0.01$.

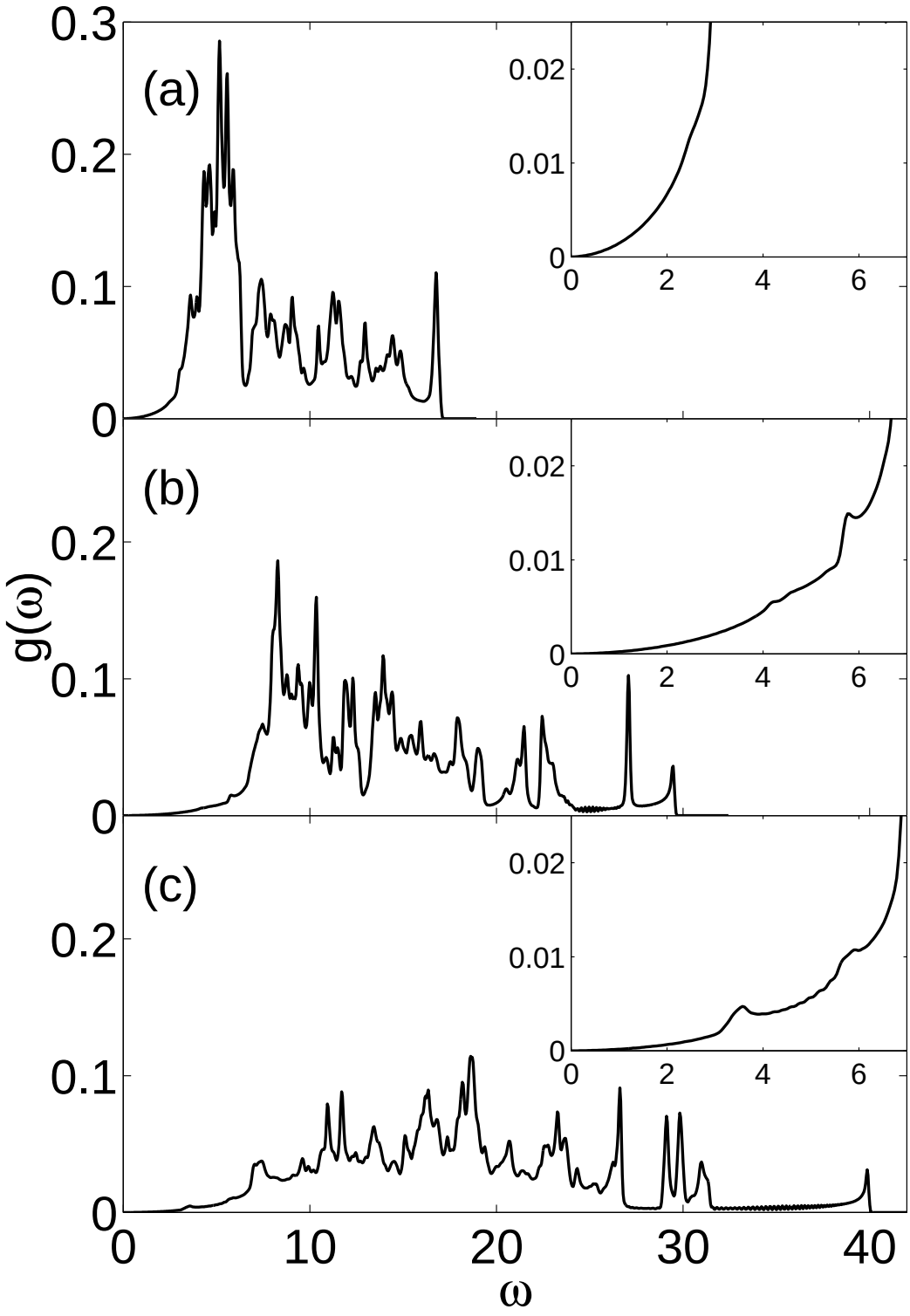


FIG. 6. Vibrational densities of states calculated by normal-mode analysis for the $\sigma$-phase structure at different pressures: (a) $P = -4.74$, (b) $P = 0$, (c) $P = 9.49$. The insets show the low-frequency parts of the corresponding spectra.

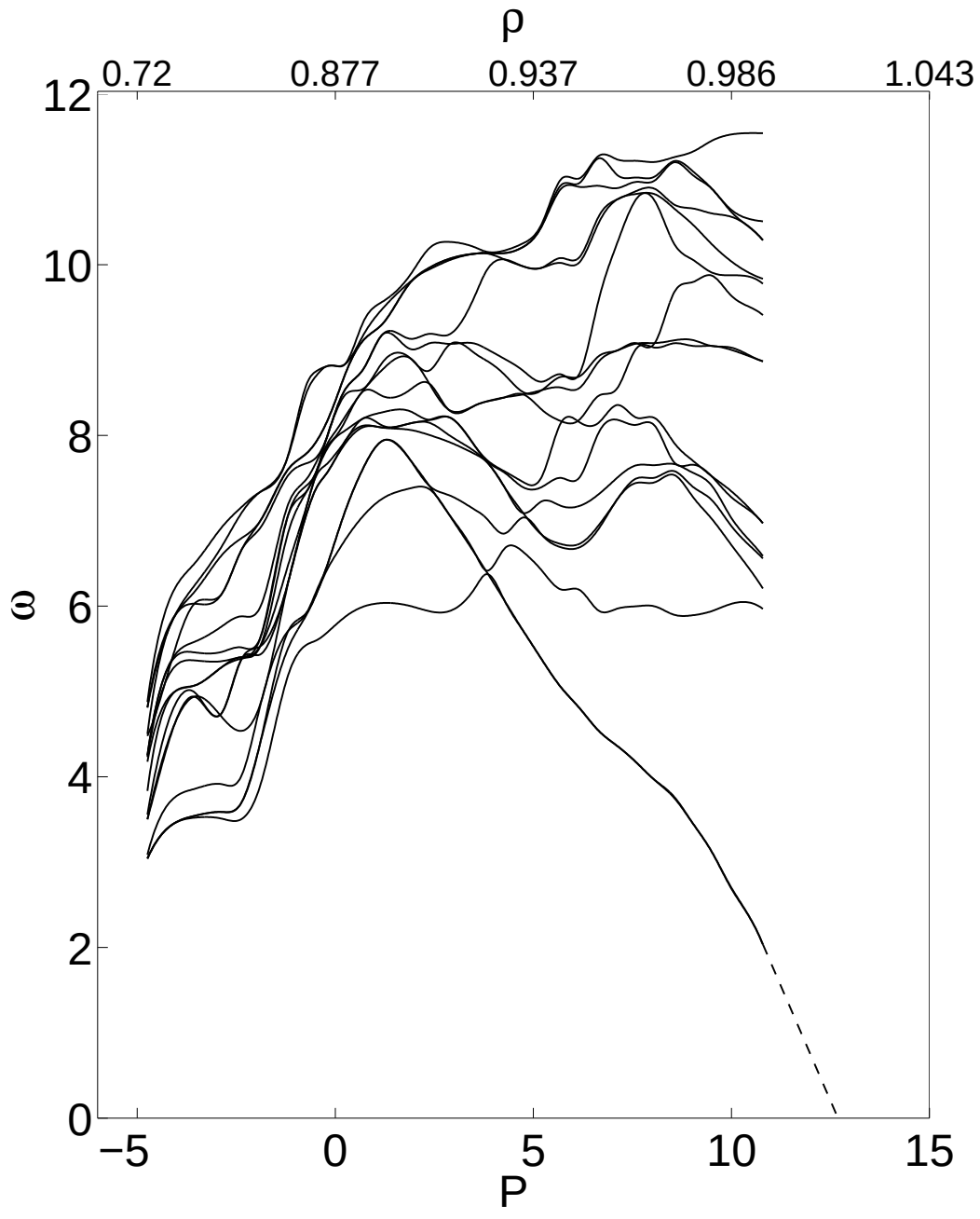


FIG. 7. Frequency of the low-frequency modes at the point Γ vs pressure. The dashed line shows a linear extrapolation of the lowest-frequency curve.

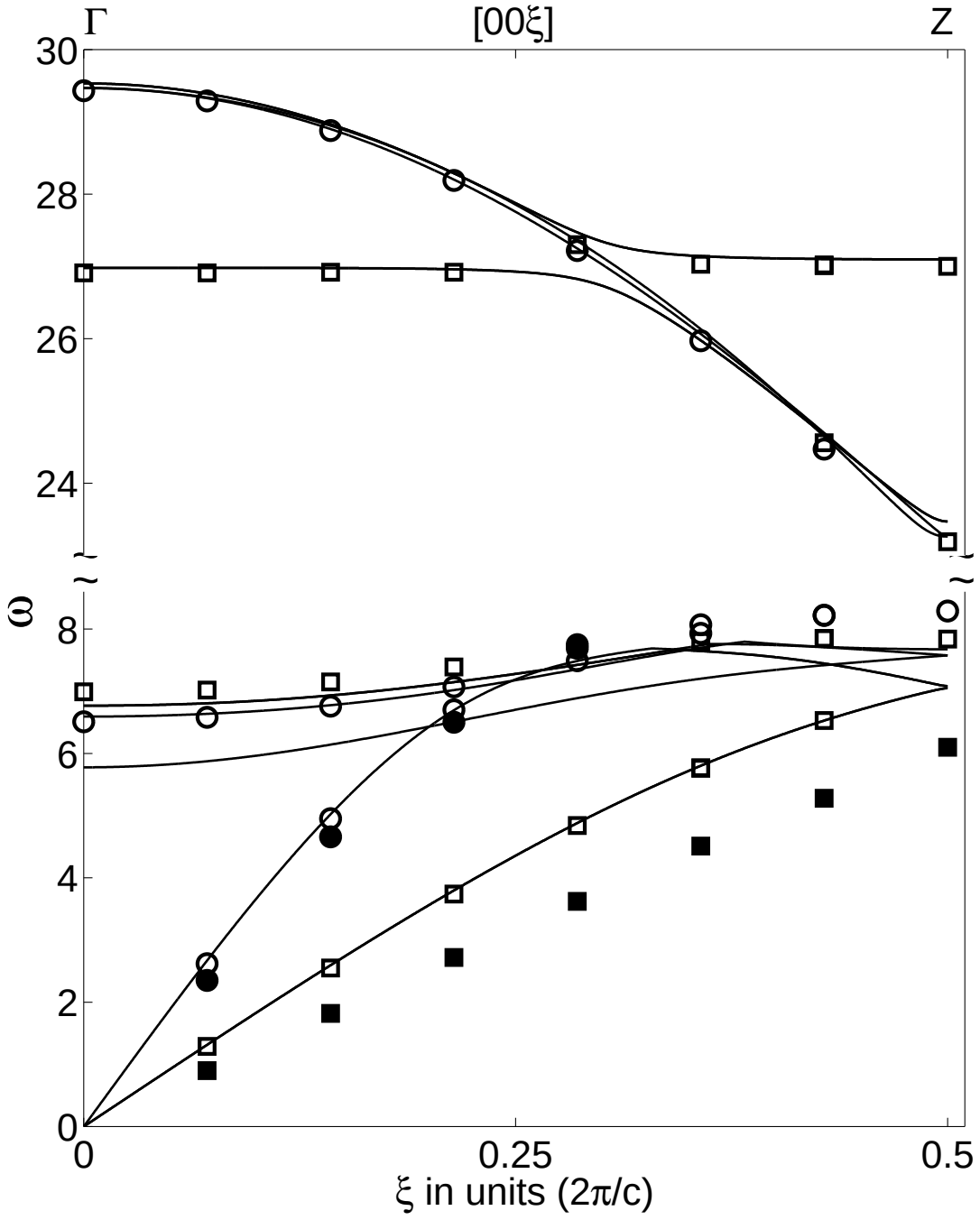


FIG. 8. Some phonon-dispersion curves calculated by a normal-mode analysis in the harmonic approximation (solid lines) and derived from the spectra of longitudinal and transverse particle-current autocorrelation functions (symbols) for the $\sigma$-phase structure. ○: longitudinal phonons; □: transverse phonons at $T = 0.01$. ●: longitudinal phonons; ■: transverse phonons at $T = 0.8$. The linear size of the symbols is approximately equal to the width of the spectral peaks. The direction of the wavevector $\mathbf{Q} = [0, 0, \xi]$, ΓZ, is parallel to the $c$-axis.

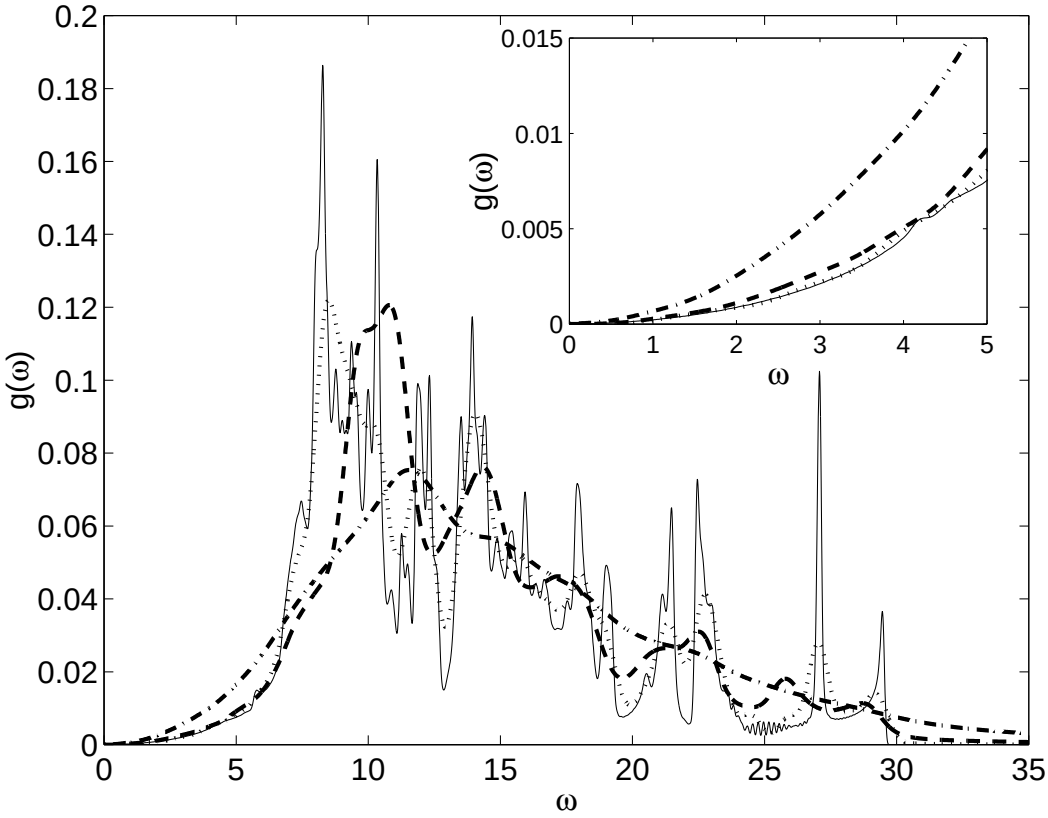


FIG. 9. Vibrational densities of states calculated by normal-mode analysis (solid line) and from the velocity autocorrelation function at different temperatures (broken lines) for the $\sigma$-phase structure. Dotted line: $T = 0.01$, dashed line: $T = 0.2$, dashed-dotted line: $T = 0.8$. The inset shows the low-frequency part of the spectrum

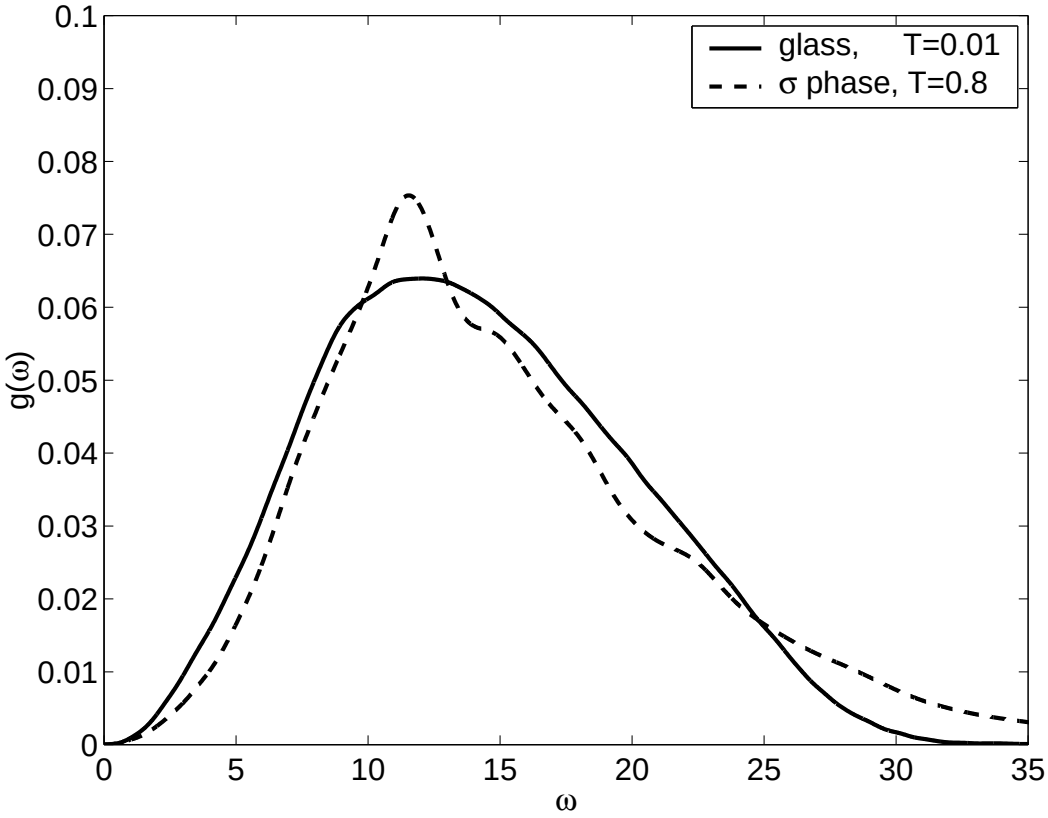


FIG. 10. Vibrational densities of states calculated from the velocity autocorrelation function for the $\sigma$-phase structure and the corresponding glass at the reduced temperatures shown. Both results are obtained at the same density $\rho = 0.8771$.